Turkish Journal of Chemistry

Volume 48 | Number 1 Article 13

2-21-2024

Palladium (0) nanoparticles distributed on lanthanum (III) oxide as an effective catalyst for the methanolysis of hydrazine-borane to produce hydrogen

Adem RÜZGAR
aruzgar@yyu.edu.tr

Lokman ŞENER
lokmansener93@gmail.com

Yaşar KARATAŞ
ykaratas@yyu.edu.tr

Mehmet GÜLCAN
mehmetgulcan65@gmail.com

TÜBİTAK

Turkish Journal of Chemistry

http://journals.tubitak.gov.tr/chem/

Research Article

Turk J Chem
(2024) 48: 137-151
© TÜBİTAK
doi:10.55730/1300-0527.3646

Palladium (0) nanoparticles distributed on lanthanum (III) oxide as an effective catalyst for the methanolysis of hydrazine-borane to produce hydrogen

Adem RÜZGAR, Lokman ŞENER, Yaşar KARATAŞ, Mehmet GÜLCAN*
Department of Chemistry, Faculty of Science, Van Yüzüncü Yil University, Van, Turkiye

Received: 10.08.2023 • **Accepted/Published Online:** 03.01.2024 • **Final Version:** 21.02.2024

Abstract: Pd (0) nanoparticles (NPs) distributed on lanthanum (III) oxide were ex situ generated from the reduction of Pd^{2+} ions using $NaBH_4$ as reducing agent. The Pd/La_2O_3 displayed good catalytic activity in H_2(g) releasing from the hydrazine-borane (HB) methanolysis reaction and it was identified by advanced techniques. Pd/La_2O_3 was found to be an active catalyst procuring three equiv. H_2(g) per mole of HB. The results from TEM images represent the formation of Pd (0) NPs with an average particle size of 1.94 ± 0.1 nm on the surface of La_2O_3. Moreover, Pd/La_2O_3 with various Pd loadings were prepared and tested as catalyst in the methanolysis reaction to find the optimum metal loading on La_2O_3 support. The highest H_2 formation rate was achieved with 3.0 wt% Pd. Pd/La_2O_3 catalyst exhibited a turnover frequency (TOF) value of 24.4 mol H_2 mol Pd^{-1} min^{-1} in the reaction conditions. Additionally, the effect of different catalyst concentrations and temperatures on the reaction kinetics for the methanolysis of HB catalyzed by Pd/La_2O_3.

Key words: Hydrazine-borane, hydrogen, methanolysis, nanoparticles, palladium

1. Introduction

Today, one of the primary objectives for all developed countries is to achieve sustainable economic growth and development. This shared goal has led to an exponential increase in the world's energy needs day by day. This rising demand for energy has unpredictably driven up the reliance on fossil fuels over the past few centuries. The use of fossil fuels not only results in water, soil, and air pollution but also poses a significant threat to human health. Moreover, it contributes to multifaceted global issues such as global warming, impacting the entire planet. Apart from these detrimental aspects, the production, transportation, and storage of fossil fuels are both expensive and hazardous. In response to these challenges associated with fossil fuels, numerous research and practical studies are underway, focusing on "alternative energy sources" [1-3]. Among these, hydrogen energy, often referred to as the energy source of the new century, stands out as a leading subject in these investigations [4-12].

Hydrogen, the lightest element, is a colorless, odorless, tasteless, flammable diatomic gas under standard conditions. One of the most important features of hydrogen gas is that it can be obtained from both inexhaustible (renewable) and fossil (nonrenewable) fuels. In addition, during the production and consumption of hydrogen; harmful wastes and chemical transformations encountered in production/consumption processes of fossil fuels are not observed. Therefore, hydrogen emerges as an energy source offering several sought-after features, including environmental friendliness, health benefits, economic viability, and ease of production [13-16]. Despite these advantages, when the quantitative distribution of energy sources that are widely used today is examined, it becomes apparent that hydrogen has not yet achieved widespread adoption as an energy source. When analyzing the obstacles hindering the widespread use of hydrogen as a substitute for conventional energy sources, it becomes evident that the most significant challenges revolve around creating efficient, safe, and cost-effective storage and transportation capabilities [17-18]. Additionally, with growing interest in reducing greenhouse gas emissions, renewable energy sources are gaining momentum as clean options for producing hydrogen as an energy carrier, devoid of carbon emissions. Renewable hydrogen serves as a bridge between renewable energy sources and the modernization of energy supply, transportation, industry, and renewable energy exports. Given hydrogen's versatility in direct use as fuel (pure H_2 or fuel mixtures) and conversion into other liquid or gaseous fuels, it can be argued that a hydrogen-based energy system offers greater durability compared to traditional fossil fuel-based systems [19-21].

* Correspondence: mehmetgulcan65@gmail.com

Hydrogen can be stored in various forms, including high-pressure gaseous, liquid, metal, or chemical hydrides. Storing hydrogen as a gas in high-pressure vessels or as a liquid at cryogenic temperatures poses serious environmental, safety, and cost issues. These challenges have spurred increased research and applications related to materials capable of storing hydrogen in the solid phase. Materials such as carbon nanotubes [22-24], metal hydrides and amine boranes [25-26], nanomaterials [27], and organometallic structures [28] are among those explored. Among these materials, amine-boranes and their derivatives have come to the forefront due to their stable structures, high hydrogen content per unit volume, being economical and environmentally friendly and have been the subject of many studies [29-35]. Within these derivative compounds, hydrazine-borane ($N_2H_4BH_3$, HB) has captured researchers' attention as a promising boron-based compound, boasting high hydrogen content (15.4 wt%) with four protic (N-H) hydrogens compared to three hydrogen (B-H) hydrides [36-44]. Research on HB has revealed its advantages, such as being solid at room temperature, water solubility, environmental nontoxicity, and stability against spontaneous hydrolysis, similar to other amine-boranes. Additionally, it has been specifically identified to possess a high gravimetric hydrogen density. Hydrogen stored in HB can be released through pyrolysis [45], hydrolysis [46] (1), and methanolysis [47] (2) reactions. However, the most promising approach for hydrogen production from HB involves complete dehydrogenation, wherein the BH_3 group undergoes hydrolysis, selectively separating N_2H_4 into N_2 and H_2 (3). Nevertheless, to maximize the efficiency of HB as a hydrogen storage material, undesired decomposition of N_2H_4 into NH_3 and N_2 (4) should be avoided. This undesired catalytic decomposition not only reduces the produced amount of H_2 but also generates NH_3, which can have a toxic effect on fuel cells. Studies have shown that these reaction pathways largely depend on catalyst design and reaction conditions. In this context, using a basic catalyst support and operating in a highly alkaline solution environment selectively advances the catalytic reaction in the desired direction [48-49].

$$N_2H_4BH_3\ (s) + 3H_2O\ (l) \rightarrow N_2H_4\ (aq) + H_3BO_3\ (l) + 3H_2\ (g) \quad (1)$$
$$N_2H_4BH_3\ (s) + 4CH_3OH\ (l) \rightarrow N_2H_5B(OCH_3)_4\ (aq) + 3H_2\ (g) \quad (2)$$
$$N_2H_4\ (aq) \rightarrow N_2\ (g) + 2H_2\ (g) \quad (3)$$
$$3N_2H_4\ (aq) \rightarrow 4NH_3\ (g) + N_2\ (g) \quad (4)$$

Two main problems encountered during the hydrolysis of amine-borane (AB) are that the hydrogen stored in the NH_3 group within the structure cannot be completely liberated under hydrolysis conditions, and NH_3 can have a poisoning effect on the catalyst at high substrate concentrations. On the other hand, these problems encountered during the hydrolysis of AB are not experienced in the hydrogen production from HB. In addition to considering the mechanistic properties of the catalytic reaction, it is possible to find out the hydrogens in the N_2H_4 group in the structure of HB in the specifically conducted hydrogen generation processes. In these selectively carried out reactions, dehydrogenation of 1 mole of $N_2H_4BH_3$ yields H_2 and N_2 in a mole ratio of 5:1. Due to the aforementioned advantages, studies aiming to produce hydrogen from HB through both hydrolysis and methanolysis have gained attention. The hydrolysis reaction can be conducted under relatively milder conditions, yielding satisfactory hydrogen evolution efficiency. However, there is an issue related to the inherent instability of HB against self-hydrolysis. In the alcoholysis reaction of HB, it has been observed that HB is more stable in methanol and does not undergo self-methanolysis. This suggests that effective hydrogen evolution from HB can be achieved in the presence of a suitable catalyst [50-52].

Research aimed at developing hydrogen production processes from HB via methanolysis has highlighted the indispensable need for suitable nanocatalysts to achieve fast, efficient, and controllable reaction environments. Nanocatalysts possess distinct physical and chemical properties compared to metal ingots, making them of great interest in recent years [53-60]. Metal nanocatalysts can show high efficiency and selectivity in catalytic reactions where metal ingots are not active. The main reason for the high catalytic efficiency they show in the reactions is the increase in the number of catalytically effective atoms on their surfaces despite the reduction in particle sizes [61-64].

Despite the positive properties mentioned above, metal nanoparticles (NPs) are kinetically unstable against the formation of metal nuggets and aggregation due to their high surface energies. Such agglomerations that will occur in the catalyst system can shorten the catalyst's lifespan and reduce reaction efficiency. To prevent this undesirable situation, in other words, to keep the nanocatalysts colloidally stable in the solution environment, suitable stabilizing groups have been used. Carbon-based materials, metal oxides, metal-organic lattice structures, polymers, and zeolites are among these groups [65-68].

The key parameters in HB dehydrogenation include the presence of a selective and active catalyst capable of decomposing both the BH_3 and N_2H_4 groups within the HB structure, as well as the development of support systems to prevent catalyst aggregation. The objective is to create efficient catalyst systems by combining rhodium, ruthenium, iridium, nickel, platinum, palladium with metals such as cobalt and copper, along with distinctive support supplies [69-79].

Rare earth elements (REE) are widely recognized for their unique chemical structures and exceptional catalytic, magnetic, and electronic properties, making them valuable in various industries and biotechnological applications. Lanthanum oxide (La_2O_3), among REE oxides, finds applications in sensors, electronic and luminescent devices, fuel cells, magnetic data storage, antimicrobial agents, catalysis, automobiles, water treatment, phosphate removal, and biomedical research [80-83]. With a bandgap ranging from 4.3 eV to 5.8 eV, La_2O_3 is a semiconductor material with the largest bandgap among REE oxides. It crystallizes in a hexagonal system structure with the *P3m1* space group and has a low photon energy of about 400 cm^{-1}, making it an excellent host matrix when doped with metals or other metal oxides [84-86].

In our study, we prepared La_2O_3-supported palladium nanoparticles (Pd NPs)—Pd/La_2O_3—for the methanolysis-based dehydrogenation of HB, and assessed the efficiency of the catalyst under mild reaction conditions. Characterization using powder X-ray diffraction (P-XRD), X-ray photoelectron spectroscopy (XPS), scanning electron microscopy (SEM), SEM-elemental mapping, transmission electron microscopy (TEM), high-resolution TEM (HRTEM), and inductively coupled plasma optical emission spectroscopy (ICP-OES) confirmed that Pd (0) NPs were well spread on the surface of La_2O_3. Pd/La_2O_3 exhibited good catalytic activity in the methanolysis of HB, with an initial turnover frequency (TOF) of 24.4 mol H_2 mol Pd^{-1} min^{-1} at 25 ± 0.1 °C, marking it as the second heterogeneous catalytic system ever reported for HB methanolysis. Furthermore, stability and durability experiments revealed that the Pd/La_2O_3 catalyst maintained its catalytic efficiency and activity to a great extent even after the 5th cycle, highlighting its high reusability and stability as a heterogeneous catalyst for HB methanolysis.

2. Experimental

2.1. Synthesis of La_2O_3 supported Pd (0) NPs

To synthesize the Pd/La_2O_3 catalyst, we first prepared a 5-mL solution containing 3% by weight Pd metal (11.22 mg, 42.1 μmol) using $Pd(NO_3)_2{\cdot}2H_2O$ salt. To this solution prepared using deionized water, 150 mg of La_2O_3 was added and the mixture was stirred at 750 rpm for 3 h. After stirring, an excess amount of $NaBH_4$ was added dropwise to reduce Pd(II) to Pd(0), (with an estimated metal/$NaBH_4$ molar ratio of 15). Once the bubbling completely ceased, indicating complete reduction of Pd(II) to Pd(0), the resulting product was filtered and washed with deionized water (3 × 20 mL) for purification. Finally, the Pd/La_2O_3 catalyst obtained from these processes was dried under appropriate conditions (Scheme).

2.2. Catalytic activity in the HB methanolysis

The main method used to assess the catalytic efficiency of Pd/La_2O_3 in the methanolysis of HB is to measure the gas formation rate. For this purpose, it was attempted to determine the catalytic efficiency by volumetrically measuring gas formation rate in different parameters. A graduated glass cylinder, resembling a gas burette, was used to determine the volume of H_2 gas produced during HB methanolysis. This involved periodically monitoring the displacement of water in the graduated cylinder due to the released H_2 gas [87]. Temperature regulation was achieved by circulating water in the system, where a 50 mL single-necked reaction balloon was positioned on a magnetic stirrer. Gas volume released was determined by measuring the volumetric displacement of water in the graduated cylinder, placed on a jacketed Schlenk, designed for temperature regulation. The necessary graphs were generated accordingly. Following the experimental setup, 100 mg (25.8 μmol, 4.69 mM) of Pd/La_2O_3 catalyst was placed on the Schlenk apparatus set at 298 K, and then 4 mL of dried methanol was added. The mouth of the jacketed Schlenk, whose temperature was controlled by means of a circulator, was sealed to prevent gas escape, and the system was stirred for about 15 min until it reached equilibrium. Subsequently, 46 mg of HB dissolved in 1 mL of dried methanol was injected into the experimental setup, maintaining a fixed stirring speed of 750 rpm. Finally, the volume (mL) of gas released due to HB methanolysis was recorded against time (min), and the corresponding graphs were plotted.

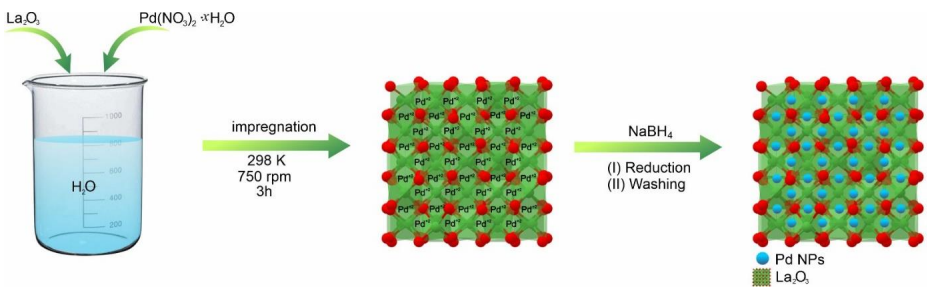

Scheme. Schematic presentation of the synthesis of Pd/La_2O_3 catalyst.

The methanol used in the experimental studies was dried through the following procedure: Methanol was dried by heating on iodine-activated magnesium with a magnesium loading of 0.5–5.0 g/L [88]. Small pieces of magnesium metal were introduced into methanol and refluxed for 2–3 h under a nitrogen atmosphere. The dry methanol was then cooled to room temperature and stored in an inert environment.

2.3. Determination of most effective Pd loading for Pd/La_2O_3

Various Pd-loaded samples (1.0%–4.0% by weight) were prepared to determine the most effective Pd loading for Pd/La_2O_3. These samples, each weighing 100 mg, were tested for H_2 gas release from the methanolysis of HB (46 mg, 200 mM HB) at 298 K. The highest H_2 formation rate was achieved for the catalyst sample containing 3.0 wt% Pd. Subsequently, the catalyst sample with 3.0 wt% Pd loading was used for further catalytic reactions.

2.4. Durability experiments

To assess the catalytic reusability and durability of the Pd/La_2O_3 catalyst in the methanolysis of HB at room temperature, a specific amount of the catalyst was used to prepare a 5-mL solution (100 mg, 25.8 μmol, 4.69 mM). This solution, along with 200 mM HB, was employed in a series of experiments. After each experiment, once the targeted reaction was complete, an equal amount of HB was reintroduced to the reaction medium. The durability data for the Pd/La_2O_3 catalyst in the methanolysis of HB was recorded as a percentage.

3. Results and discussion

P-XRD, XPS, TEM, HRTEM, SEM, and ICP-OES analyses were conducted on the Pd/La_2O_3 catalyst to assess its structural and morphological properties. Initially, ICP-OES analysis was utilized to determine the distribution of Pd metal content on La_2O_3, revealing a Pd content of 2.7 ± 0.1 wt%. It is important to note that the theoretical metal content of the Pd/La_2O_3 catalyst was designed to contain 3.0 wt% Pd.

SEM analysis was performed to examine the distribution of Pd NPs on the La_2O_3 surface, which served as a support, and to characterize the surface morphology (Figures 1a–1c). To achieve the desired image quality, the sample of the Pd/La_2O_3 catalyst was coated with gold for approximately 100 s. SEM images and corresponding elemental mapping of Pd/La_2O_3 confirmed the presence of La, O, and Pd elements and the uniform dispersion of Pd NPs within the Pd/La_2O_3 catalyst. On the other hand, Pd exhibited a homogeneous distribution similar to other elements but with a lower density. This is also associated with the contribution of Pd (0) NPs at lower concentrations compared to other elements. As confirmed by the SEM elemental mapping in the obtained SEM images, it is noticed that Pd NPs were extremely uniformly distributed on La_2O_3 surface (Figures 1d–1f).

The preservation of an intact La_2O_3 structure after the deposition of Pd NPs was confirmed by the Bragg peaks of the La_2O_3 support shown in the P-XRD patterns of the La_2O_3 structure and the Pd/ La2O3 catalyst (Figure 2). The major XRD diffraction peaks of La_2O_3 corresponded well with the hexagonal La_2O_3 phase (JCPDS: 05-0602). The Bragg diffraction peaks at 2θ values of 15.7°, 27.2°, 28.2°, 39.5°, 48.7°, 55.4°, 56.5°, 59.1°, 64.1°, 69.7°, and 77.7° are respectively indexed to the crystal planes (100), (002), (101), (102), (110), (103), (112), (201), (202), (203), and (210) of La_2O_3 [89-90]. The absence of Bragg peaks attributable to Pd NPs indicated a low (<5% by weight) loading of Pd NPs on the host La_2O_3 surface. Additionally, some changes in charge distribution and electrostatic fields were observed due to the interaction of Pd NPs and electrophilic structures on the surface with framework atoms. These changes were largely attributed to the decrease in the intensity of Bragg peaks observed in the Pd/La_2O_3 catalyst [64].

XPS analysis was employed to identify the elements present in the Pd/La_2O_3 catalyst and elucidate its surface characteristics. The survey analysis of the Pd/La_2O_3 catalyst in Figure 3a revealed the presence of the Pd element along with the framework elements of La_2O_3. High-resolution spectrum of Pd 3d bands displayed two prominent peaks at 334.4 and 339.9 eV corresponding to metallic Pd $3d_{5/2}$ and Pd $3d_{3/2}$, respectively [32,64,91]. This indicates reduction of Pd^{2+} ions used as a precursor and the existence of metallic Pd in the Pd (0) form within the catalyst sample. Additionally, small peaks observed at 342.4 eV and 336.2 eV were associated with Pd–O $3d_{3/2}$ and Pd–O $3d_{5/2}$ bonds, respectively [92].

TEM images of the Pd/La_2O_3 catalyst with 3.0 wt% Pd loading are presented in Figure 4. These images reveal that Pd (0) NPs are uniformly distributed on the surface of La_2O_3 at various magnifications. A particle size histogram was generated by counting more than 100 nontouching particles, determining the mean diameter of Pd (0) NPs as 1.94 ± 0.1 nm. The TEM–EDX spectrum of the Pd/La_2O_3 catalyst (2.7 ± 0.1 wt% Pd) in Figure 5c confirms the presence of La, O, and Pd as the only elements, consistent with XPS analysis in Figure 3a. Additionally, the HRTEM image of the Pd/La_2O_3 catalyst indicates a d-spacing of 0.21 nm corresponding to the Pd (111) lattice plane (Figure 4d) [32,64,91].

Before conducting catalytic activity tests and detailed kinetic studies, we conducted two significant preliminary investigations. Firstly, the catalytic nature of La_2O_3 and Pd/La_2O_3 materials in the target catalytic reaction was compared under the same conditions to determine the net reactivity of Pd (0) nanoparticles in the methanolysis of HB. At the end of the

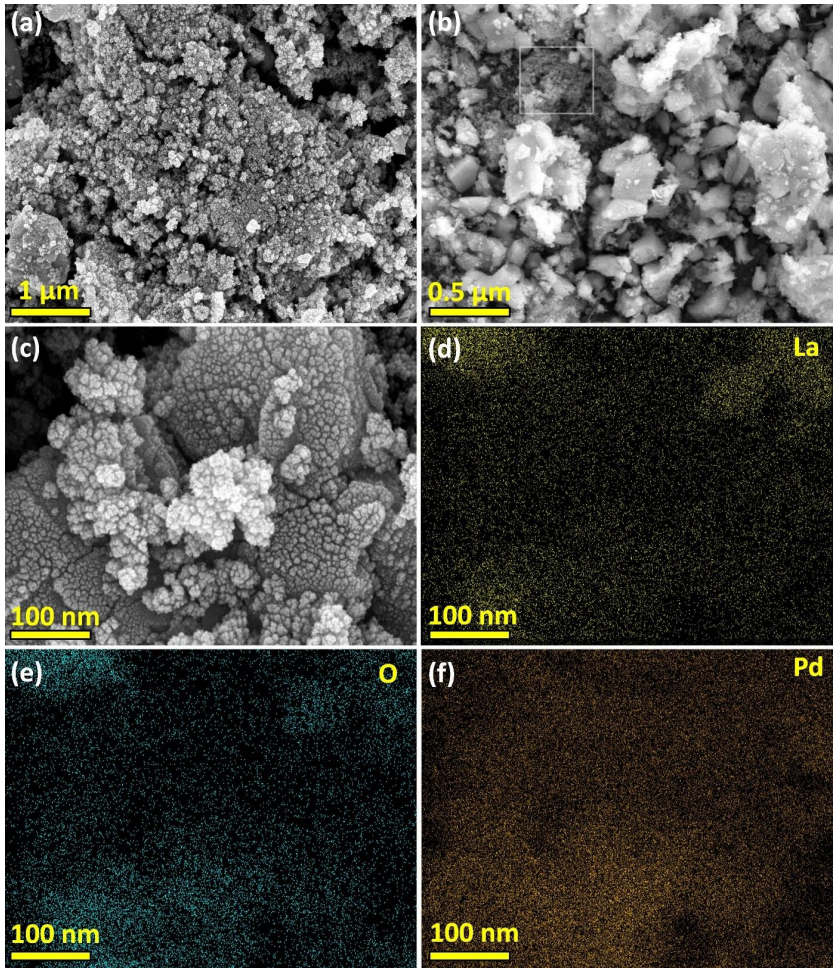

Figure 1. SEM image at different scales (a-c), along with corresponding elemental mapping La (d), O (e), and Pd (f) on the surface of the Pd/La_2O_3 catalyst.

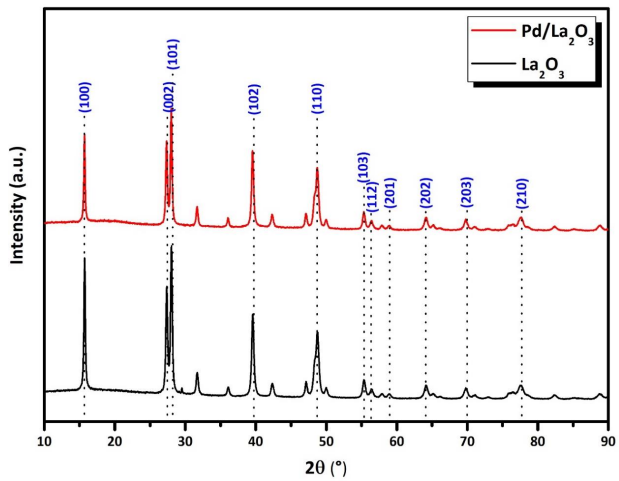

Figure 2. P-XRD patterns of the Pd/La_2O_3 catalyst and La_2O_3 solid support at $2\theta = 10°–90°$.

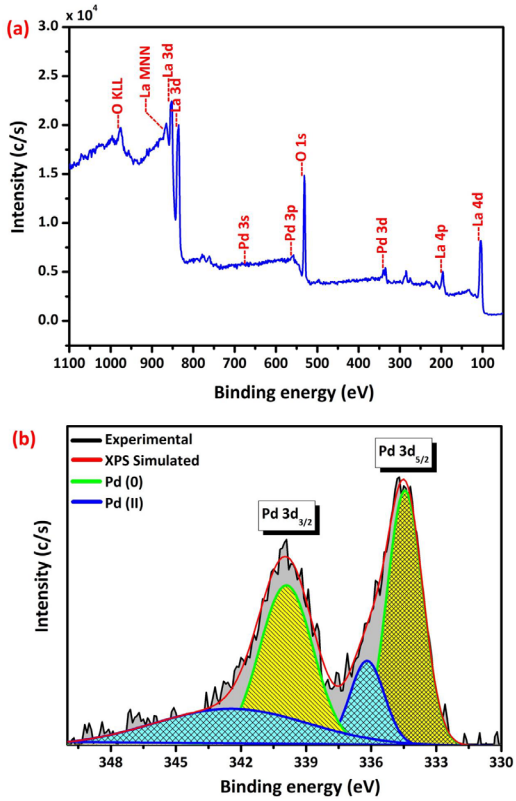

Figure 3. Survey scan (a) and Pd 3d core level XPS spectra of Pd/La_2O_3 catalyst.

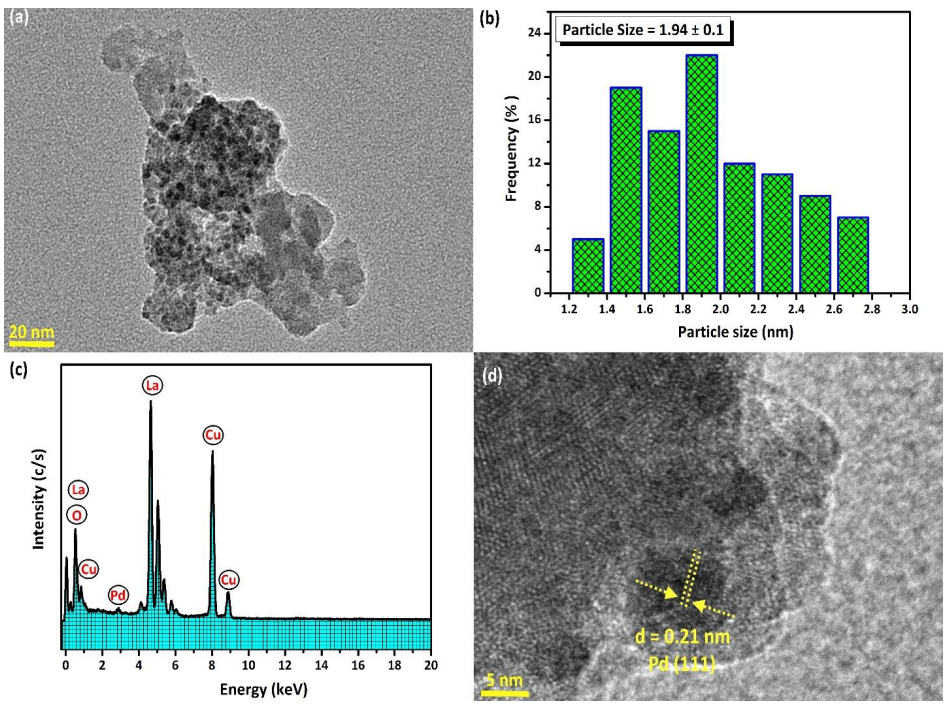

Figure 4. (a) TEM image of Pd/La_2O_3 (2.7 ± 0.1 wt % Pd) catalyst), (b) size distribution histogram for Pd (0) NPs, (c) TEM–EDX spectrum, and (d) HRTEM image of the Pd/La_2O_3 catalyst.

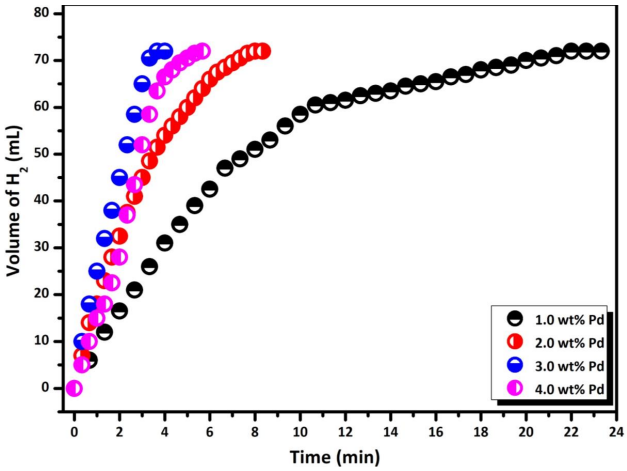

Figure 5. Graphs of released volume of gas vs. time for 200 mM HB methanolysis in different Pd loadings (1.0, 2.0, 3.0, 4.0 wt% Pd) at 298 K.

experiment, it was determined that the metal-free La_2O_3 was not catalytically active in this catalytic conversion (Figure S1). Secondly, Pd-loaded La_2O_3 samples containing varying percentages of Pd were prepared, and their catalytic activities were tested in the methanolysis of HB. Figure 5 illustrates the H_2 evolution graph from HB methanolysis catalyzed by Pd/La_2O_3 with different Pd loading ranging from 1.0% to 4.0 wt% Pd. Upon addition of the HB substrate, H_2 production commenced without an observed induction time and continued until the gas equivalent reached 3.0 in the catalytic methanolysis reaction. The sample with 3.0 wt% Pd loading was established as the most active catalyst for H_2 generation from HB methanolysis. The H_2 generation rate (TOF) of the catalyst was calculated as 24.4 mol H_2 mol Pd^{-1} min^{-1} for Pd/La_2O_3 with 3.0 wt% Pd. Higher palladium loadings resulted in a decrease in the surface area of the supporting material and failure to reach active sites of the catalyst. Therefore, Pd/La_2O_3 samples with a 3.0 wt% Pd ratio were selected as the optimum ratio for all other experiments.

Figure 6 illustrates the graphs of H_2 gas volume (mL) versus H_2 gas time (min) released when Pd/La_2O_3 is utilized as a catalyst in the methanolysis of 200 mM HB at 298 K. Based on the reaction data employing catalysts at varying concentrations, the Pd/La_2O_3 catalyst demonstrated outstanding catalytic activity across all reactions. Upon examining the graphs, it is evident that the hydrogen formation processes start without any induction period at all concentrations and continue until all HB in the solution is converted into products, indicating an almost linear methanolysis process of HB. Drawing a graph of Pd concentration versus the rate of hydrogen formation on a logarithmic scale reveals a correlation (see inset of Figure 6), showing that the HB methanolysis process using the Pd/La_2O_3 catalyst yields a straight line with a slope of approximately 2.0 concerning the Pd/La_2O_3 catalyst concentration.

A significant outcome of the study is the achievement of complete conversion of HB methanolysis within 5 min at 298 K using 2.7 ± 0.1 wt% Pd. The TOF (turnover frequency) value for the Pd/La_2O_3catalyst in HB methanolysis was calculated as 24.4 mol H_2 mol Pd^{-1} min^{-1} at 298 K, representing an important result among catalytic systems employed in HB methanolysis, as summarized in Table. Additionally, the Pd/La_2O_3 catalyst represents the second heterogeneous catalytic system used in HB methanolysis.

To assess the effect of HB concentration on the formation rate of H_2 gas released during catalytic methanolysis, catalytic studies were conducted using various HB concentrations at a constant catalyst concentration ([Pd] = 4.69 mM) and temperature (298 K). The volume of H_2 gas released in the methanolysis reactions initiated with different HB concentrations was measured at regular intervals, and a volume (mL)/time (min) graph was generated, as shown in Figure 7. Upon examination of the graph, the effect of HB concentration on the reaction's initial rate appears to be rather limited. The graph of the initial concentration of HB versus the hydrogen production rate yields a line with a slope of ≈0.8 (inset of Figure 7), indicating that HB methanolysis catalyzed by Pd/La_2O_3 proceeds kinetically by half-order with HB concentration.

So far, the reaction mechanism of HB methanolysis has not been studied extensively, similar to the AB methanolysis reaction, which has been rarely explored in the literature [95-97]. In this context, it is estimated that the reaction mechanism of HB methanolysis in the presence of the Pd/La_2O_3 catalyst can be elucidated as follows, drawing parallels with AB: (i) adsorption and activation of methanol on Pd NPs on La_2O_3, facilitating the absorption of HB molecules; (ii) scission of O–H bond in CH_3OH to produce H* and *OCH_3; (iii) attack of OCH_3 on the B atom in HB, leading to the formation of

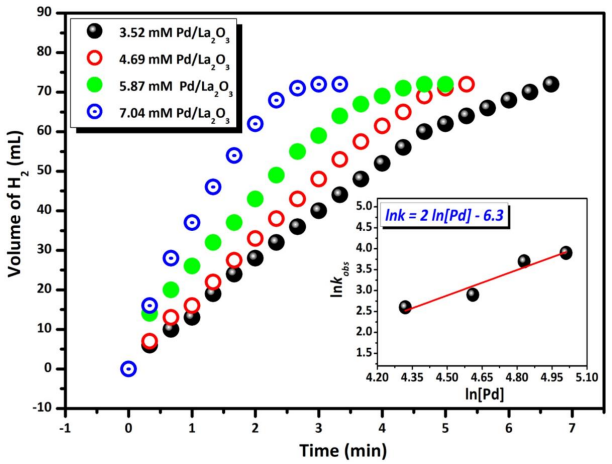

Figure 6. Graphs of the released gas volume vs. time for 200 mM HB methanolysis in different concentrations of Pd/La_2O_3 catalyst ([Pd] = 3.52, 4.69, 5.87 and 7.04 mM) at 298 K. Inset: Plot of rate of the hydrogen generation vs. palladium concentration (in logaritmic scale).

Table. Comparing thermodynamic parameters and activities of catalysts used in the formation of H_2 as a result of HB methanolysis.

Catalyst	TOF[a]	E_a[b]	T (K)	Ref.
$NiCl_2$	24.0	65	298	[93]
PVP-stabilized Ni NPs	35.6	63 ± 2	298	[50]
$PdCl_2$	NG	100.3	303	[94]
Ru NPs@*nano*-CeO_2	41.05	102.6	298	[44]
Pd/La_2O_3	**24.4**	**53.7**	**298**	**This study**

[a]*Turnover frequency, mol H_2 mol cat^{-1} min^{-1};* [b]*Activation energy (kJ/mol), NG (not given), PVP, polyvinylpyrrolidone.*

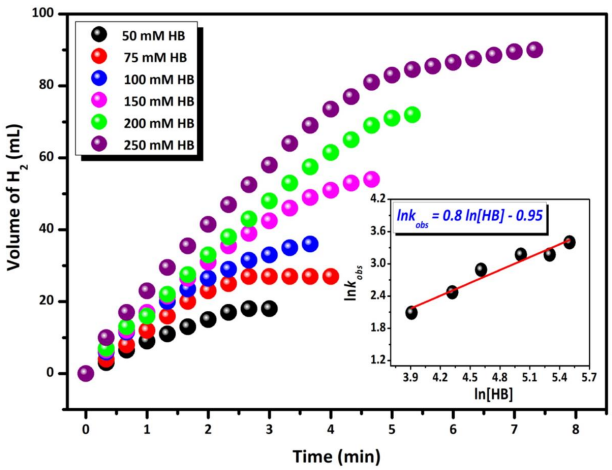

Figure 7. Graphs of released gas volume vs. time for HB methanolysis in different concentrations of HB ([HB] = 100, 150, 200, and 250 mM) at 298 K. Inset: Plot of rate of hydrogen generation vs. concentration of HB (in logaritmic scale).

$N_2H_4BH_2$–OCH_3 and another H; (iv) combination of two H to form one H_2 molecule, which then exits the catalyst surface. A similar process repeats until the other two H_2 molecules are produced (Figure 8) [96-97].

In catalytic methanolysis reactions with an HB concentration of 200 mM and a Pd/La_2O_3 catalyst amount of 100 mg (4.69 mM), the effect of temperature changes (288, 298, 308, and 318 K) on the H_2 formation rate was measured at regular intervals. The volume/time graph obtained is shown in Figure 9. Upon examination of the obtained graph, it is observed that catalytic methanolysis is completed rapidly, even at temperatures below room temperature, and the H_2 formation rate changes in direct proportion to the temperature. For the methanolysis of HB catalyzed by the Pd/La_2O_3 catalyst, activation parameters such as E_a, $\Delta H^{\#}$, and $\Delta S^{\#}$ were calculated from temperature-dependent graphs drawn using Arrhenius and Eyring kinetic equations (Figures S2 and S3). The slope of the linear part of each hydrogen generation versus time plot at different temperatures indicates the reaction rate constant kobs of the methanolysis reaction. While the Arrhenius curve (Figure 9, inset) was used for the activation energy (E_a), which was found to be 53.66 kJ/mol (Figure S2), the Eyring curve was used to calculate the activation enthalpy ($\Delta H^{\#}$ = 51 kJ/mol) and activation entropy ($\Delta S^{\#}$ = 48.5 J/mol×K) values (Figure S3). This E_a value is the lowest calculated Ea for HB methanolysis compared to the catalytic systems summarized in Table.

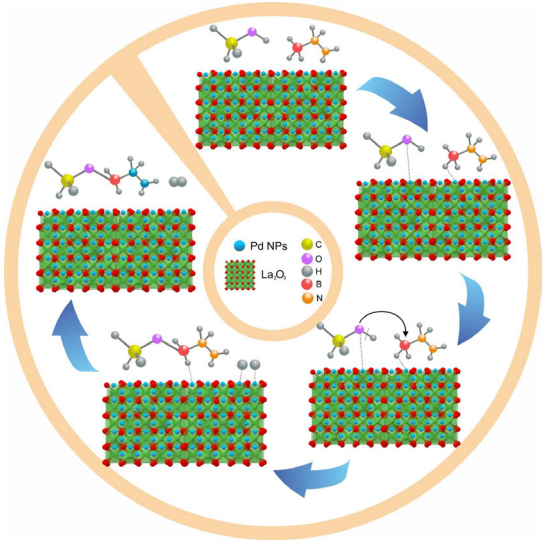

Figure 8. Plausible mechanism of HB methanolysis catalyzed with Pd/La_2O_3.

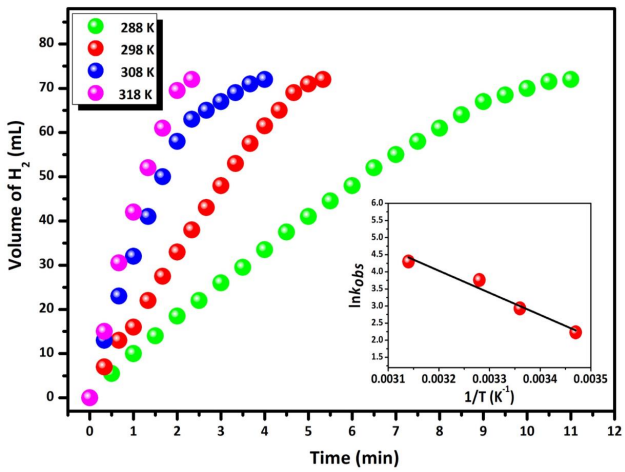

Figure 9. Graphs of the gas volume vs. time for the methanolysis of HB starting with 200 mM HB plus 100.0 mg Pd/La_2O_3 catalyst (4.69 mM) at different temperatures (288, 298, 308, and 318 K).

After detailed kinetic studies, the recyclability performance of the Pd/La_2O_3 catalyst in hydrogen production from HB methanolysis was investigated (Figure 10). The study aimed to determine the catalytic recycling durability of the prepared Pd/La_2O_3 catalyst, when all of the HB was converted to the product, more HB was added to the solution medium and the catalyst efficiency in repeated catalytic reactions was determined. At the end of the methanolysis reactions continued for up to 5 cycles, it was determined that the Pd/La_2O_3 catalyst exhibited extremely high stability and durability, preserving 81% of the initial yield and achieving approximately 99% conversion even in the 5th cycle. Some reduction in catalytic activity can be attributed to the closure of the catalyst's active surfaces by methanolysis reaction products or to the increase in particle size or aggregation of Pd (0) NPs. This is also evident in the TEM image of the product isolated as a result of the 5th catalytic cycle, with clusters circled in Figure 10b.

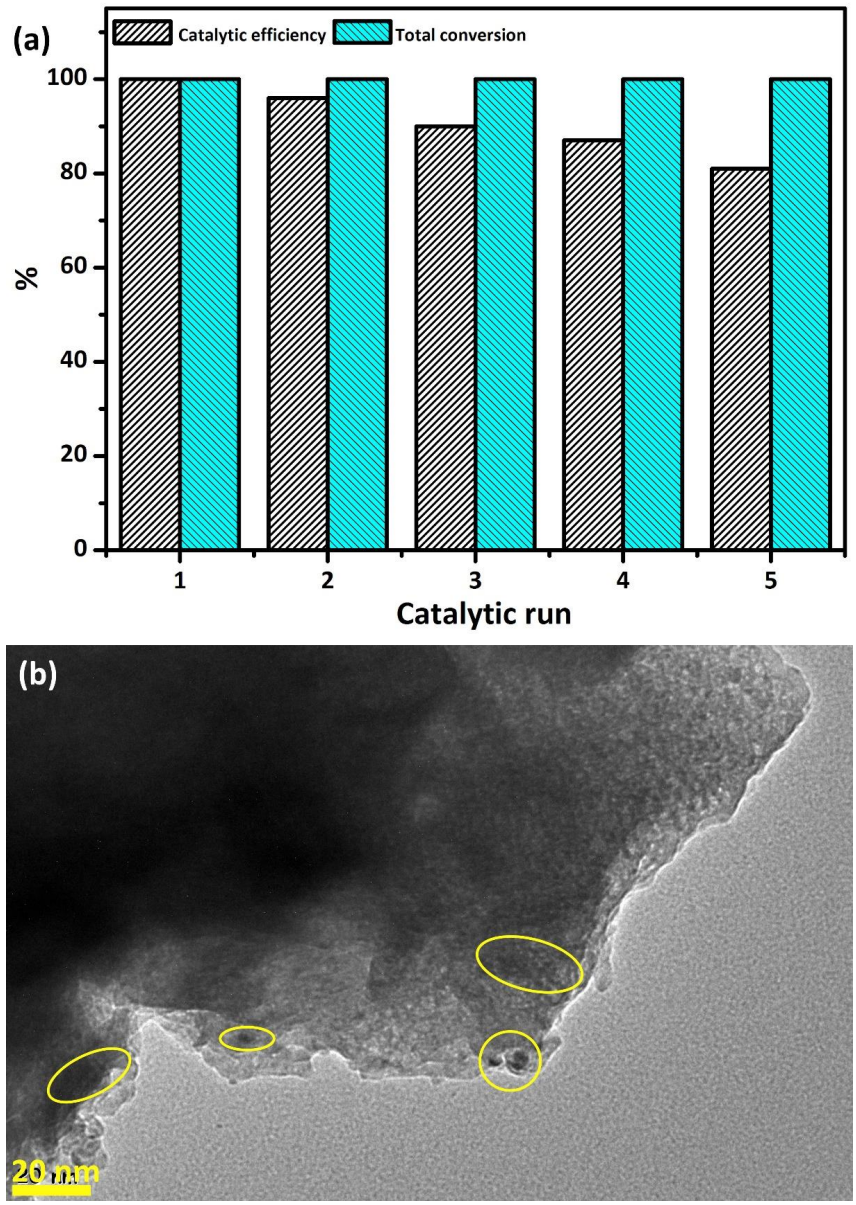

Figure 10. (a) Time plots of catalytic methanolysis of HB by up to 5 recycle for the Pd/La_2O_3 catalyst at 298 K and, (b) TEM image of Pd/La_2O_3 catalyst obtained after the 5th catalytic recycle.

4. Conclusions

The prepared Pd/La_2O_3 catalyst yielded significant results in the hydrogen production from HB methanolysis:

(i) Using an easy and reproducible impregnation-reduction technique, we synthesized Pd(0) NPs supported on La_2O_3;

(ii) To elucidate the structural and morphological characteristics of Pd/La_2O_3 catalyst, we employed SEM, SEM-Elemental Mapping, XRD, XPS, ICP-OES, TEM, HRTEM and TEM-EDX techniques;

(iii) Compared with the initial turnover frequency of the second heterogeneous system used for the HB methanolysis, the Pd/La_2O_3 catalyst exhibits a catalytic efficiency of 24.4 min^{-1} at 298 K;

(iv) The properties of Pd/La_2O_3, characterized by high recyclability and excellent resistance to aggregation, have been verified. The catalyst demonstrates remarkable stability during catalytic recycles, retaining 81% of the initial yield and exceeding 99% in the 5th recycling;

(v) It has been demonstrated that the methanolysis of HB in the presence of the Pd/La_2O_3 catalyst follows second and ≈first-order kinetics with respect to Pd and HB concentrations, respectively. This conclusion is drawn from detailed kinetic studies that are dependent on Pd/La_2O_3 catalyst and HB concentrations. For the HB methanolysis catalyzed by the Pd/La_2O_3 catalyst, temperature-dependent kinetic studies were conducted, leading to anticipated values for the activation energy (E_a), enthalpy of activation ($\Delta H^{\#}$), and entropy of activation ($\Delta S^{\#}$) parameters (E_a = 53.66 kJ/mol, $\Delta H^{\#}$ = 51 kJ/mol, $\Delta S^{\#}$ = 48.5 J/mol×K). Notably, the calculated E_a value is the lowest reported for HB methanolysis compared to other catalytic systems in the literature.

References

[1] Di L, Zhang J, Zhang X, Xia G, Hua Y et al. Cold plasma enhanced preparation of high performance PdRu/C formic acid dehydrogenation catalysts. International Journal of Hydrogen Energy 2021; 46: 37836-37846. https://doi.org/10.1016/j.ijhydene.2021.09.036

[2] Kumar A, Kumar J, Bhaskar T. High surface area biochar from Sargassum tenerrimum as potential catalyst support for selective phenol hydrogenation. Environmental Research 2020; 186: 109533. https://doi.org/10.1016/j.envres.2020.109533.

[3] Brack P, Dann SE, Wijayantha KGU. Heterogeneous and homogenous catalysts for hydrogen generation by hydrolysis of aqueous sodium borohydride ($NaBH_4$) solutions. Energy Science & Engineering 2015; 3: 74-88. https://doi.org/10.1002/ese3.67

[4] Schlapbach L, Zuttel A. Hydrogen-storage materials for mobile applications. Nature 2001; 414: 353-358. https://doi.org/10.1038/35104634

[5] Eberle U, Felderhoff M, Schüth F. Chemical and physical solutions for hydrogen storage. Angewandte Chemie International Edition 2009; 48: 6608-6630. https://doi.org/10.1002/anie.200806293

[6] Holladay JD, Wang Y, Jones E. Review of developments in portable hydrogen production using microreactor technology. Chemical Reviews 2004; 104: 4767-90. https://doi.org/10.1021/cr020721b

[7] Hill AK, Torrente Murciano L. In-situ H_2 production via low temperature decomposition of ammonia: insights into the role of cesium as a promoter. International Journal of Hydrogen Energy 2014; 39: 7646-54. https://doi.org/10.1016/j.ijhydene.2014.03.043

[8] Li S, Sun J, Guan J. Strategies to improve electrocatalytic and photocatalytic performance of two-dimensional materials for hydrogen evolution reaction. Chinese Journal of Catalysis 2021; 42: 511-56. https://doi.org/10.1016/S1872-2067(20)63693-2

[9] Wang X, Zheng Y, Sheng W, Xu ZJ, Jaroniec M et al. Strategies for design of electrocatalysts for hydrogen evolution under alkaline conditions. Materials Today 2020; 36: 125-38. https://doi.org/10.1016/j.mattod.2019.12.003

[10] Su P, Pei W, Wang X, Ma Y, Jiang Q et al. Exceptional electrochemical HER performance with enhanced electron transfer between Ru nanoparticles and single atoms dispersed on a carbon substrate. Angewandte Chemie International Edition 2021; 60: 16044-50. https://doi.org/10.1002/anie.202103557

[11] Boyjoo M, Wang M, Pareek VK, Liu J, Jaroniec M. Synthesis and applications of porous non-silica metal oxide submicrospheres. Chemical Society Reviews 2016; 45: 6013-47. https://doi.org/10.1039/C6CS00060F

[12] Gong F, Liu M, Ye S, Gong L, Zeng G et al. All-pH stable sandwich-structured MoO_2/MoS_2/C hollow nanoreactors for enhanced electrochemical hydrogen evolution. Advanced Functional Materials 2021; 31: 2101715. https://doi.org/10.1002/adfm.202101715

[13] Davoodabadi A, Mahmoudi A, Ghasemi H. The potential of hydrogen hydrate as a future hydrogen storage medium. İScience 2020; 24: 101907. https://doi.org/10.1016/j.isci.2020.101907

[14] Hanley ES, Deane JP, Gallachóir BPO. The role of hydrogen in low carbon energy futures–A review of existing perspectives. Renewable and Sustainable Energy Reviews 2018; 82: 3027-3045. https://doi.org/10.1016/j.rser.2017.10.034

[15] Seh ZW, Kibsgaard J, Dickens CF, Chorkendorff I, Nørskov JK et al. Combining theory and experiment in electrocatalysis: insights into materials design. Science 2017; 146: 355. https://10.1126/science.aad4998

[16] Wang Z, Li Q, Xu H, Dahl Petersen C, Yang Q et al. Controllable etching of MoS_2 basal planes for enhanced hydrogen evolution through the formation of active edge sites. Nano Energy 2018; 49: 634. https://doi.org/10.1016/j.nanoen.2018.04.067

[17] Li J, Ren X, Lv H, Wang Y, Li Y et al. Highly efficient hydro-gen production from hydrolysis of ammonia borane over nano-structured Cu@ $CuCoO_x$ supported on graphene oxide. Journal of Hazardous Materials 2020; 391: 122199. https://doi.org/10.1016/j.jhazmat.2020.122199

[18] Gulcan M, Karatas Y. Synthesized polyvidone-stabilized Rh(0) nanoparticles catalyzed the hydrolytic dehydrogenation of methylamine-borane in ambient conditions. New Journal of Chemistry 2017; 41: 11839. https://doi.org/10.1039/C7NJ02481A

[19] Acar C, Dincer I. Review and evaluation of hydrogen production options for better environment. Journal of Cleaner Production 2019; 218: 835-849. https://doi.org/10.1016/j.jclepro.2019.02.046

[20] Abdalla AM, Hossain S, Nisfindy OB, Azad AT, Dawood M et al. Hydrogen production, storage, transportation and key challenges with applications: a review. Energy Conversion and Management 2018; 165: 602-627. https://doi.org/10.1016/j.enconman.2018.03.088

[21] Dawood F, Anda M, Shafiullah GM. Hydrogen production for energy: An overview. International Journal of Hydrogen Energy 2020; 45: 3847-3869. https://doi.org/10.1016/j.ijhydene.2019.12.059

[22] Liu C, Fan YY, Liu M, Cong H, Cheng HM et al. Hydrogen storage in single-walled carbon nanotubes at room temperature. Science 1999; 286: 1127-1129. https://10.1126/science.286.5442.11

[23] Sharma A. Hydrogen storage in platinum loaded single-walled carbon nanotubes, International Journal of Hydrogen Energy 2020; 45: 23966-23970. https://doi.org/10.1016/j.ijhydene.2019.09.025

[24] Sawant SV, Banerjee S, Patwardhan AW, Joshi JB, Dasgupta K. Synthesis of boron and nitrogen co-doped carbon nanotubes and their application in hydrogen storage. International Journal of Hydrogen Energy 2020; 45: 13406-13413. https://doi.org/10.1016/j.ijhydene.2020.03.019

[25] Malahayati M, Yufita E, Ismail I, Mursal M, Jalil Z. Hydrogen desorption properties of MgH_2 + 10 wt% SiO_2 + 5 wt% Ni prepared by planetary ball milling. Bulletin of Chemical Reaction Engineering & Catalysis 2021; 16: 280-285. https://10.9767/bcrec.16.2.10220.280-285

[26] Rahwanto A, Ismail I, Nurmalita N, Mustanir, Jalil Z. Nanoscale Ni as a catalyst in MgH_2 for hydrogen storage material. Journal of Physics: Conference Series 2021; 1882. https://10.1088/1742-6596/1882/1/012010

[27] Banerjee P, Chandrakumar KRS, Das GP. Exploring adsorption and desorption characteristics of molecular hydrogen on neutral and charged Mg nanoclusters: a first principles study. Chemical Physics 2016; 469: 123-131. https://doi.org/10.1016/j.chemphys.2016.02.004

[28] Broom DP, Webb CJ, Fanourgakis GS, Froudakis GE, Trikalitis PN et al. Concepts for improving hydrogen storage in nanoporous materials. International Journal of Hydrogen Energy 2019; 44: 7768-7779. https://doi.org/10.1016/j.ijhydene.2019.01.224

[29] Yıldırım R, Gülcan M. H_2 production from the hydrolytic dehydrogenation of methylamine-borane catalyzed by sulfonated reduced graphene oxide-aided synthesis of ruthenium nanoparticles. International Journal of Hydrogen Energy 2021; 46: 32523-32535. https://doi.org/10.1016/j.ijhydene.2021.07.096

[30] Yang X, Sun JK, Kitta M, Pang H, Xu Q. Encapsulating Highly catalytically active metal nanoclusters inside porous organic cages. Nature Catalysis 2018; 1: 214–220. https://doi.org/10.1038/s41929-018-0030-8

[31] Zhu QL, Zhong DC, Demirci UB, Xu Q. Controlled synthesis of ultrafine surfactant-free nipt nanocatalysts toward efficient and complete hydrogen generation from hydrazine borane at room temperature. ACS Catalysis 2014; 4: 4261-4268. https://doi.org/10.1021/cs501329c

[32] Karatas Y, Gülcan M, Çelebi M, Zahmakiran M. Pd (0) nanoparticles decorated on graphene nanosheets (GNS): synthesis, definition and testing of the catalytic performance in the methanolysis of ammonia borane at room conditions. ChemistrySelect 2017; 2: 9628-9635. https://doi.org/10.1002/slct.201701616

[33] Aijaz A, Karkamkar A, Choi YJ, Tsumori N, Rönnebro E et al. Immobilizing highly catalytically active pt nanoparticles inside the pores of metal-organic framework: a double solvents approach. Journal of American Chemical Society 2012; 134: 13926–13929. https://doi.org/10.1021/ja3043905

[34] Wan C, Sun L, Xu L, Cheng DG, Chen F et al. Novel NiPt alloy nanoparticle decorated 2D layered g-C_3N_4 nanosheets: a highly efficient catalyst for hydrogen generation from hydrous hydrazine. Journal of Material Chemistry A 2019; 7: 8798–8804. https://doi.org/10.1039/C9TA01535C

[35] Konus N, Karatas Y, Gulcan M. In situ formed ruthenium(0) nanoparticles supported on TiO_2 catalyzed hydrogen generation from aqueous ammonia-borane solution at room temper-ature under air. Synthesis and Reactivity in Inorganic, Metal-Organic, and Nano-Metal Chemistry 2016; 46: 534-542. https://doi.org/10.1080/15533174.2014.988808

[36] Zhu QL, Xu Q. Liquid organic and inorganic chemical hydrides for high-capacity hydrogen storage. Energy & Environmental Science 2015; 8: 478-512. https://doi.org/10.1039/C4EE03690E

[37] Yadav M, Xu Q. Liquid-phase chemical hydrogen storage materials. Energy & Environmental Science 2012; 5: 9698-9725. https://doi.org/10.1039/C2EE22937D

[38] Hugle T, Kuhnel MF, Lentz D. Hydrazine borane: a promising hydrogen storage material. Journal of American Chemical Society 2009; 131: 7444-7447. https://doi.org/10.1021/ja9013437

[39] Moury R, Demirci UB. Hydrazine borane and hydrazinidoboranes as chemical hydrogen storage materials. Energies 2015; 8: 3118-3141. https://doi.org/10.3390/en8043118

[40] Aziza WB, Petit JF, Demirci UB, Xu Q, Miele P. Bimetallic nickel-based nanocatalysts for hydrogen generation from aqueous hydrazine borane: investigation of iron, cobalt and palladium as the second metal. International Journal of Hydrogen Energy 2014; 39: 16919-16926. https://doi.org/10.1016/j.ijhydene.2014.06.169

[41] Hannauer J, Akdim O, Demirci UB, Geantet C, Herrmann JM et al. High-extent dehydrogenation of hydrazine borane $N_2H_4BH_3$ by hydrolysis of BH_3 and decomposition of N_2H_4. Energy & Environmental Science 2011; 4: 3355-3358. https://doi.org/10.1039/C1EE01886H

[42] Zhang ZJ, Lu ZH, Tan HL, Chen XS, Yao QL. CeOx-modified RhNi nanoparticles grown on rGO as highly efficient catalysts for complete hydrogen generation from hydrazine borane and hydrazine. Journal of Material Chemistry 2015; 3: 23520-23529. https://doi.org/10.1039/C5TA06197K

[43] Li SJ, Wang HL, Wulan BR, Zhang XB, Yan JM et al. Complete dehydrogenation of $N_2H_4BH_3$ over noble-metal-free $Ni_{0.5}Fe_{0.5}$–CeO_x/MIL-101 with high activity and 100% H_2 selectivity. Advanced Energy Materials 2018; 8: 1800625. https://doi.org/10.1002/aenm.201800625

[44] Karatas Y, Gülcan M, Şen F. Catalytic methanolysis and hydrolysis of hydrazine-borane with monodisperse Ru NPs@nano-CeO2 catalyst for hydrogen generation at room temperature. International Journal of Hydrogen Energy 2019; 44: 13432-13442. https://doi.org/10.1016/j.ijhydene.2019.04.012

[45] Hügle T, Kühnel MF, Lentz D. Hydrazine borane: A promising hydrogen storage material. Journal of American Chemical Society 2009; 131: 7444–7446. https://doi.org/10.1021/ja9013437

[46] Huang M, Yao Q, Feng G, Zou H, Lu ZH. Nickel–ceria nanowires embedded in microporous silica: controllable synthesis, formation mechanism, and catalytic applications. Inorganic Chemistry 2020; 59: 5781–5790. https://doi.org/10.1021/acs.inorgchem.0c00600

[47] Zahmakiran M, Ozkar S. Transition metal nanoparticles in catalysis for the hydrogen generation from the hydrolysis of ammonia-borane. Topics in Catalysis 2013; 56: 1171–1183. https://doi.org/10.1007/s11244-013-0083-5

[48] Moury R, Moussa G, Demirci UB, Hannauer J, Bernard S et al. Hydrazine borane: synthesis, characterization, and application prospects in chemical hydrogen storage. Physical Chemistry Chemical Physics 2012; 14: 1768–1777. https://doi.org/10.1039/C2CP23403C

[49] Hannauer J, Akdim O, Demirci UB, Geantet C, Herrmann JM et al. High-extent dehydrogenation of hydrazine borane $N_2H_4BH_3$ by hydrolysis of BH_3 and decomposition of N_2H_4. Energy & Environmental Science 2011; 4: 3355–3358. https://doi.org/10.1039/C1EE01886H

[50] Özhava D, Kılıçaslan NZ, Özkar S. PVP-stabilized nickel(0) nanoparticles as catalyst in hydrogen generation from the methanolysis of hydrazine borane or ammonia borane. Applied Catalysis B: Environmental 2015; 162: 573-582. https://doi.org/10.1016/j.apcatb.2014.07.033

[51] Yao QL, Lu ZH, Wang YQ, Chen X, Feng G. Synergetic catalysis of non-noble bimetallic Cu–Co nanoparticles embedded in SiO_2 nanospheres in hydrolytic dehydrogenation of ammonia borane. Journal of Physical Chemistry C 2015; 119: 14167-14174. https://doi.org/10.1021/acs.jpcc.5b02403

[52] Şencanlı S, Karahan S, Özkar S. Poly(4-styrenesulfonic acid-co-maleic acid) stabilized nickel(0) nanoparticles: highly active and cost effective catalyst in hydrogen generation from the hydrolysis of hydrazine borane. International Journal of Hydrogen Energy 2013; 38: 14693-14703. https://doi.org/10.1016/j.ijhydene.2013.09.060

[53] Li J, Hong X, Wang Y, Luo Y, Huang P et al. Encapsulated cobalt nanoparticles as a recoverable catalyst for the hydrolysis of sodium borohydride. Energy Storage Materials 2020; 27: 187–197. https://doi.org/10.1016/j.ensm.2020.01.011

[54] Wang C, Li L, Yu W, Lu ZM, Zhang XH et al. Regulation of d-band electrons to enhance the activity of Co-based non-noble bimetallic catalysts for hydrolysis of ammonia borane, ACS Sustainable Chemistry & Engineering 2020; 8: 8256-8266. https://doi.org/10.1021/acssuschemeng.0c01475

[55] Li YT, Zhang XL, Peng ZK, Liu P, Zheng XC. Hierarchical porous g-C_3N_4 coupled ultrafine RuNi alloys as extremely active catalyst for the hydrolytic dehydrogenation of ammonia borane. ACS Sustainable Chemistry & Engineering 2020; 8: 8458–8468. https://doi.org/10.1021/acssuschemeng.0c03009

[56] Cui C, Liu Y, Mehdi S, Wen W, Zhou B et al. Enhancing effect of Fe-doping on the activity of nano Ni catalyst towards evolution from NH_3BH_3. Applied Catalysis B: Environmental 2020; 265: 118612. https://doi.org/10.1016/j.apcatb.2020.118612

[57] Rej S, Hsia CF, Chen TY, Lin FC, Huang JS et al. Facet-dependent and light-assisted efficient hydrogen evolution from ammonia borane using gold-palladium core-shell nanocatalysts. Angewandte Chemie International Edition 2016; 55: 7222–7226. https://doi.org/10.1002/anie.201603021

[58] Rej S, Mascaretti L, Santiago EY, Tomanec O, Kment S et al. Determining plasmonic hot electron and photothermal effects during H2 evolution with TiN-Pt nanohybrids. ACS Catalysis 2020; 10: 5261–5271. https://doi.org/10.1021/acscatal.0c00343

[59] Fu LL, Zhang DF, Yang Z, Chen TW, Zhai J. PtAuCo trimetallic nanoalloys as highly efficient catalysts toward dehydrogenation of ammonia borane. ACS Sustainable Chemistry & Engineering 2020; 8: 3734–3742. https://doi.org/10.1021/acssuschemeng.9b06865

[60] Li X, Zhang C, Luo M, Yao Q, Lu ZH. Ultrafine Rh nanoparticles confined by nitrogen-rich covalent organic framework for methanolysis of ammonia borane. Inorganic Chemistry Frontiers 2020; 7: 1298–1306. https://doi.org/10.1039/D0QI00073F

[61] Ding R, Chen Q, Luo Q, Zhou L, Wang Y et al. Salt template-assisted in situ construction of Ru nanoclusters and porous carbon: excellent catalysts towards hydrogen evolution, ammonia-borane hydrolysis, and 4-nitrophenol reduction. Green Chemistry 2020; 22: 835–842. https://doi.org/10.1039/C9GC03986D

[62] Yao QL, Yang KK, Nie WD, Li YX, Lu ZH. Highly efficient hydrogen generation from hydrazine borane via a MoO_x promoted NiPd nanocatalyst. Renewable Energy 2020; 147: 2024-2031. https://doi.org/10.1016/j.renene.2019.09.144

[63] Bhattacharjee I, Bhunya S, Paul A. Frustrated Lewis acid base-pair-catalyzed amine-borane dehydrogenation. Inorganic Chemistry 2020; 59: 1046–1056. https://doi.org/10.1021/acs.inorgchem.9b02561

[64] Çelebi M, Rüzgar A, Karataş Y, Gülcan M. Manganese oxide octahedral molecular sieves stabilized Rh nanoparticles for the hydrogen production from the ethylenediamine-bisborane hydrolysis. International Journal of Hydrogen Energy 2022; 47: 16494-16506. https://doi.org/10.1016/j.ijhydene.2022.03.127

[65] Zahmakıran M, Özkar S. Metal nanoparticles in liquid phase catalysis; from recent advances to future goals. Nanoscale 2011; 3: 3462-3481. https://doi.org/10.1039/C1NR10201J

[66] Yadav M, Akita T, Tsumori N, Xu Q. Strong metalemolecular support interaction (SMMSI): amine-functionalized gold nanoparticles encapsulated in silica nanospheres highly active for catalytic decomposition of formic acid. Journal of Materials Chemistry 2012; 22: 12582-6. https://doi.org/10.1039/C2JM31309J

[67] Yıldırım R, Karatas Y¸ Demirci UB, Gülcan M. Fabrication and characterization of copper nanoparticles anchored on sulfonated reduced graphene oxide as effective catalyst for the reduction of Thioflavine-T cationic dye in aqueous medium. Materials Chemistry and Physics 2022; 275: 125212. https://doi.org/10.1016/j.matchemphys.2021.125212

[68] Rüzgar A, Karatas Y, Gülcan M. Synthesis and characterization of Pd0 nanoparticles supported over hydroxyapatite nanospheres for potential application as a promising catalyst for nitrophenol reduction. Heliyon 2023; 9: e21517. https://doi.org/10.1016/j.heliyon.2023.e21517

[69] Yurderi M, Top T, Bulut A, Kanberoglu GS, Kaya M et al. Complete dehydrogenation of hydrazine borane on manganese oxide nanorod supported Ni@Ir core–shell nanoparticles. Inorganic Chemistry 2020; 59: 9728-9738. https://doi.org/10.1021/acs.inorgchem.0c00965

[70] Lu ZH, Yao Q, Zhang Z, Yang Y, Chen X. Nanocatalysts for hydrogen generation from ammonia borane and hydrazine borane. Journal of Nanomaterials 2014; 11: 729029. https://doi.org/10.1155/2014/729029

[71] Tunç N, Abay B, Rakap M. Hydrogen generation from of hydrolytic dehydrogenation of hydrazine borane by poly(N-vinyl-2-pyrrolidone)-stabilized palladium nanoparticles. Journal of Power Sources 2015; 299: 403-407. https://doi.org/10.1016/j.jpowsour.2015.09.032

[72] Yang K, Yao Q, Huang W, Chen X, Lu ZH. Enhanced catalytic activity of NiM (M = Cr, Mo, W) nanoparticles for hydrogen evolution from ammonia borane and hydrazine borane. International Journal of Hydrogen Energy 2017; 42: 6840-6850. https://doi.org/10.1016/j.ijhydene.2016.12.029

[73] Kanat M, Karatas Y, Gülcan M, Anıl B. Preparation and detailed characterization of zirconia nanopowder supported rhodium (0) nanoparticles for hydrogen production from the methanolysis of methylamine-borane in room conditions. International Journal of Hydrogen Energy 2018; 43: 22548-22556. https://doi.org/10.1016/j.ijhydene.2018.10.130

[74] Yao Q, Lu ZH, Zhang R, Zhang S, Chen X et al. A noble metal-free nanocatalyst for highly efficient and complete hydrogen evolution from N2H4BH3. Journal of Material Chemistry A 2018; 6: 4386-4393. https://doi.org/10.1039/C7TA10886A

[75] Zhang Z, Lu ZH, Chen X. Ultrafine Ni-Pt alloy nanoparticles grown on graphene as highly efficient catalyst for complete hydrogen generation from hydrazine borane. ACS Sustainable Chemistry & Engineering 2015; 3: 1255-61. https://doi.org/10.1021/acssuschemeng.5b00250

[76] Çakanyıldırım Ç, Petit E, Demirci UB, Moury R, Petit JF et al. Gain insight into the catalytic dehydrogenation of hydrazine borane in water. International Journal of Hydrogen Energy 2012; 37: 15983-15991. https://doi.org/10.1016/j.ijhydene.2012.08.032

[77] Rakap M, Abay B, Tunç N. Hydrolysis of ammonia borane and hydrazine borane by poly(N-vinyl-2-pyrrolidone)-stabilized CoPd nanoparticles for chemical hydrogen storage. Turkish Journal of Chemistry 2017; 41: 221-232. https://doi.org/10.3906/kim-1604-44

[78] Singh SK, Lu ZH, Xu Q. Temperature-induced enhancement of catalytic performance in selective hydrogen generation from hydrous hydrazine with Ni-based nanocatalysts for chemical hydrogen storage. European Journal of Inorganic Chemistry 2011; 14: 2232. https://doi.org/10.1002/ejic.201100083

[79] Singh SK, Xu Q. Complete conversion of hydrous hydrazine to hydrogen at room temperature for chemical hydrogen storage. Journal of American Chemical Society 2009; 131: 18032. https://doi.org/10.1021/ja908037t

[80] Balusamy B, Tastan BE, Ergen SF, Uyar T, Tekinay T. Toxicity of lanthanum oxide (La_2O_3) nanoparticles in aquatic environments. Environmental Science: Processes & Impacts 2015; 17: 1265. https://doi.org/10.1039/C5EM00035A

[81] Balusamy B, Kandhasamy YG, Senthamizhan A, Chandrasekaran G, Subramanian MS et al. Characterization and bacterial toxicity of lanthanum oxide bulk and nanoparticles. Journal of Rare Earths 2012; 30 (12): 1298–1302. https://doi.org/10.1016/S1002-0721(12)60224-5

[82] Zhang L, Wan L, Chang N, Liu J, Duan C et al. Removal of phosphate from water by activated carbon fiber loaded with lanthanum oxide. Journal of Hazardous Materilas 2011; 190: 848–855. https://doi.org/10.1016/j.jhazmat.2011.04.021

[83] Zhang L, Gao Y, Li M, Liu J. Expanded graphite loaded with lanthanum oxide used as a novel adsorbent for phosphate removal from water: performance and mechanism study. Environmental Technology 2015; 36 (8): 1016–1025. https://doi.org/10.1080/09593330.2014.971884

[84] Méndez M, Carvajal JJ, Cesteros Y, Marsal LF, Martínez Ferrero E et al. Photoluminescence and cathodoluminescence of Eu:La_2O_3 nanoparticles synthesized by several methods. Physics Procedia 2010; 8: 114–120. https://doi.org/10.1016/j.phpro.2010.10.021

[85] Sulaiman N, Yulizar Y, Apriandanu DOB. Eco-friendly method for synthesis of La2O3 nanoparticles using Physalis angulata leaf extract. AIP Conference Proceedings 2018; 2023: 020105. https://doi.org/10.1063/1.5064102

[86] Ghiasi M, Malekzadeh A. Synthesis, characterization and photocatalytic properties of lanthanum oxy-carbonate, lanthanum oxide and lanthanum hydroxide nanoparticles. Superlattices Microstructures 2015; 77: 295. https://doi.org/10.1016/j.spmi.2014.09.027

[87] Karatas Y, Çetin T, Akkus IN, Akinay Y, Gulcan M. Rh(0) nanoparticles impregnated on two-dimensional transitionmetal carbides, MXene, as an effective nanocatalyst forammonia-borane hydrolysis. International Journal of Energy Research 2022; 46: 11411-11423. https://doi.org/10.1002/er.7938

[88] Williams DBG, Lawton M. Drying of organic solvents: quantitative evaluation of theefficiency of several desiccants. Journal of Organic Chemistry 2010; 75: 8351–8354. https://doi.org/10.1021/jo101589h

[89] Cheraghali R, Aghazadeh M. A Simple and facile electrochemical route to synthesis of metal hydroxides and oxides ultrafine nanoparticles (M=La, Gd, Ni and Co). Analytical and Bioanalytical Electrochemistry 2016; 8: 64-77.

[90] Wu Q, Xiong J, Mei X, Zhang Y, Wei Y et al. Efficient catalysts of La2O3 nanorod-supported pt nanoparticles for soot oxidation: the role of La_2O_3-{110} facets. Industrial & Engineering Chemistry Research 2019; 58 (17): 7074–7084. https://doi.org/10.1021/acs.iecr.9b01018

[91] Gulcan M, Zahmakiran M, Özkar S. Palladium(0) nanoparticles supported on metal organic framework as highly active and reusable nanocatalyst in dehydrogenation of dimethylamine-borane. Applied Catalysis B: Environmental 2014; 147: 394-401. https://doi.org/10.1016/j.apcatb.2013.09.007

[92] Karatas Y, Çetin T, Akinay Y, Gülcan M. Synthesis and characterization of Pd doped MXene for hydrogen production from the hydrolysis of methylamine borane: Effect of cryogenic treatment. Journal of the Energy Institute 2023; 109: 101310. https://doi.org/10.1016/j.joei.2023.101310

[93] Karahan S, Zahmakiran M, Özkar S. Catalytic methanolysis of hydrazine borane: a new and efficient hydrogen generation system under mild conditions. Dalton Transactions 2012; 41: 4912–4918. https://doi.org/10.1039/C2DT11867J

[94] Goh JD, Lee HL, Chua YS. Palladium (II) chloride catalytic methanolysis of hydrazine borane for enhanced hydrogen production. Journal of Physical Science 2019; 30: 127-139. https://doi.org/10.21315/jps2019.30.s2.11

[95] Li Z, He T, Matsumura D, Miao S, Wu A et al. Atomically dispersed Pt on the surface of Ni particles: synthesis and catalytic function in hydrogen generation from aqueous ammonia-borane. ACS Catalysis 2017; 7: 6762–6769. https://doi.org/10.1021/acscatal.7b01790

[96] Kumar DR, Prabu S, Chiang KY, Oh TH. Methanolysis of ammonia borane using binder-free hierarchical Co@Ni metal-organic framework nanocolumn arrays catalyst for hydrogen generation. International Journal of Energy Research 2022; 46: 18134-18145. https://doi.org/10.1002/er.8432

[97] Liao J, Wu Y, Shao Y, Feng Y, Zhang Z et al. Ammonia borane methanolysis for hydrogen evolution on $Cu_3Mo_2O_9$/$NiMoO_4$ hollow microspheres. Chemical Engineering Journal 2022; 449: 137755. https://doi.org/10.1016/j.cej.2022.137755

Supplementary Material

Materials

Palladium (II) nitrate dihydrate ($Pd(NO_3)_2 \cdot 2H_2O$), lanthanum (III) oxide (La_2O_3), hydrazine hemisulfate salt ($H_2NNH_2 \cdot 0.5H_2SO_4$, ≥98 %), methanol ($CH_3OH$, 99 %), tetrahydrofuran (C_4H_8O, THF, 99.9 %) and sodium borohydride ($NaBH_4$, powder, ≥98.0%) purchased from Sigma-Aldrich were used as-received and without further purification. Under argon atmosphere methanol and THF were distilled using sodium-benzophenone and magnesium. A water purification system for distilled deionized water was used (Milli-Q Water Purification System). The catalytic materials isolated at the end of the synthesis were stored in a in vacuum atmosphere. Acetone was used to wash all glassware and Teflon-coated magnetic stir sticks and rinsed profusely with distilled water before drying in an oven at 393 K.

Synthesis of hydrazine-borane ($N_2H_4BH_3$, HB)

The synthesis of HB was performed as described in the literature[S1-S2]. According to the reaction in *Scheme S1*, the preparation of the HB is carried out according to the reaction of sodium borohydride with hydrazine hemisulfate salt in THF at 25 °C. The purity of the hydrazine-borane used in the experiments was determined using FT-IR, ^{1}H, and melting point analytical methods. Melting point of HB: 60.6 °C; ^{1}H-NMR (400 MHz, CH_2Cl_2-d_2) 5.1 ppm (t, 2, $N_2H_4BH_3$), 3.4 ppm (b, 2, $N_2H_4BH_3$), 1.2 ppm (t, 3, $N_2H_4BH_3$); FT-IR (selected, cm^{-1}) 3333 (s), 3220 (s), 2836 (m), 2662 (m), 2367 (m), 1622 (s), 1592 (m), 1437 (w), 1338 (m), 1157 (s), 912 (m), 750 (w). The obtained results are consistent with those of previous studies[S1-S3].

$$N_2H_4 \cdot 1/2H_2SO_4 + NaBH_4 \xrightarrow[298\ K]{THF} 2N_2H_4BH_3 + Na_2SO_4 + 2H_2$$

Scheme S1. Synthesis protocol of HB in THF at 25 °C.

Characterization techniques

The crystal information of the obtained materials was gained with a Rigaku Ultima-IV model X-ray diffraction (Cu K_a radiation, λ = 1.54 Å). The working voltage and current of the X-ray tube were 40 kV and 40 mA, respectively. The surface morphology and microstructure of the obtained catalysts were observed by using TEM and HRTEM techniques. TEM and HRTEM samples were prepared by dropping one drop of dilute suspension on a copper-coated carbon TEM grid and then drying the solvent. TEM analysis was carried out on a JEOL JEM-200CX transmission electron microscope operating at 120 kV. HRTEM analyses were run on a JEOL JEM-2010F transmission electron microscope operating at 200 kV. The 3D morphological images of samples were carried out using a Zeiss Sigma 300 model field emission scanning electron microscope (FESEM) with an energy dispersive X-ray (EDX) spectroscopy and In-Lens (SE1) detector at 10kV accelerating voltage. The surface chemistry information of the obtained catalysts was acquired on a Kratos AXIS Ultra spectrometer was employed for XPS analysis using monochromatic Al-Kα radiation (1486.6 eV, the X-ray tube working at 15 kV and 350 W, and pass energy of 23.5 eV). The C 1s photoelectron line (binding energy = 284.6 eV) was used to calibrate the binding energies of the photoelectron. The metal content in the obtained catalysts was evaluated with the inductively coupled plasma optical emission spectrometry (ICP-OES) analysis on a Perkin Elmer Optima 4300DV ICP emission spectrometer. Before ICP-OES analysis, each sample was completely dissolved in a mixture of HNO_3/HCl (1/3; v/v). Fourier-transform infrared (FT-IR) spectra were taken on a Bio-Rad-Win-IR spectrophotometer carrying out KBr discs in between 4000 and 400 cm^{-1}. NMR instrument (Bruker 400 MHz Ultrashield TM) for NMR analysis was used, which is applied deuterated dichloromethane (CH_2Cl_2-d_2) as solvent using tetramethylsilane (TMS) as internal standards.

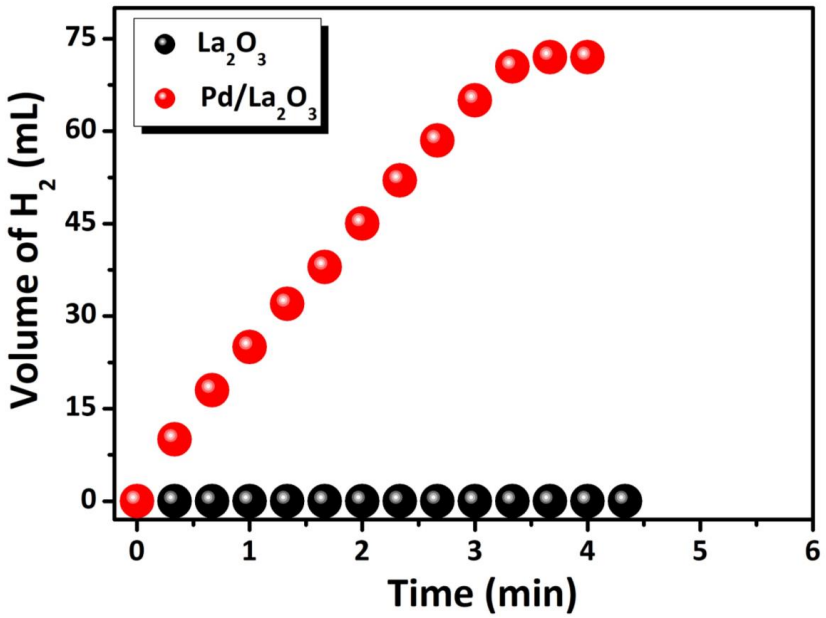

Figure S1. Graphs of released volume of gas vs. time for 200 mM HB methanolysis with La_2O_3 and Pd/La_2O_3 catalyst at 298 K.

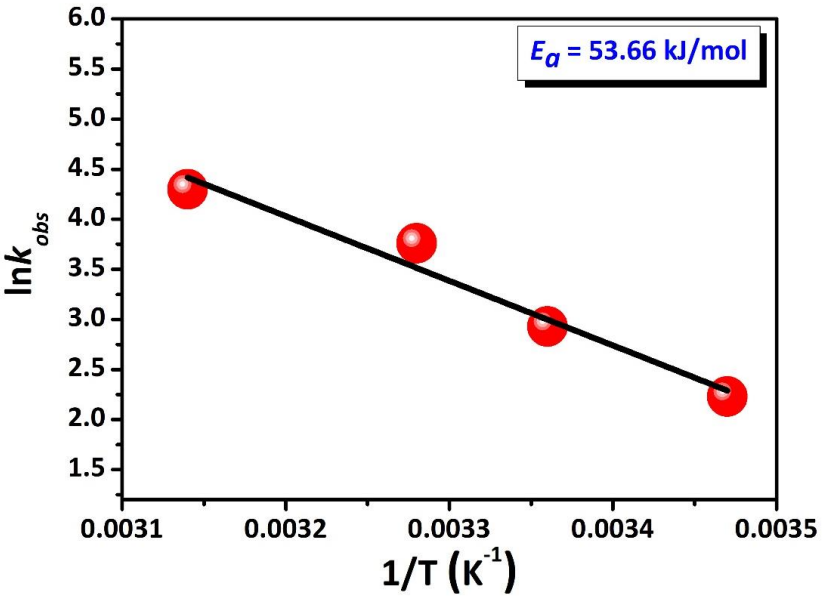

Figure S2. Arrhenius curve.

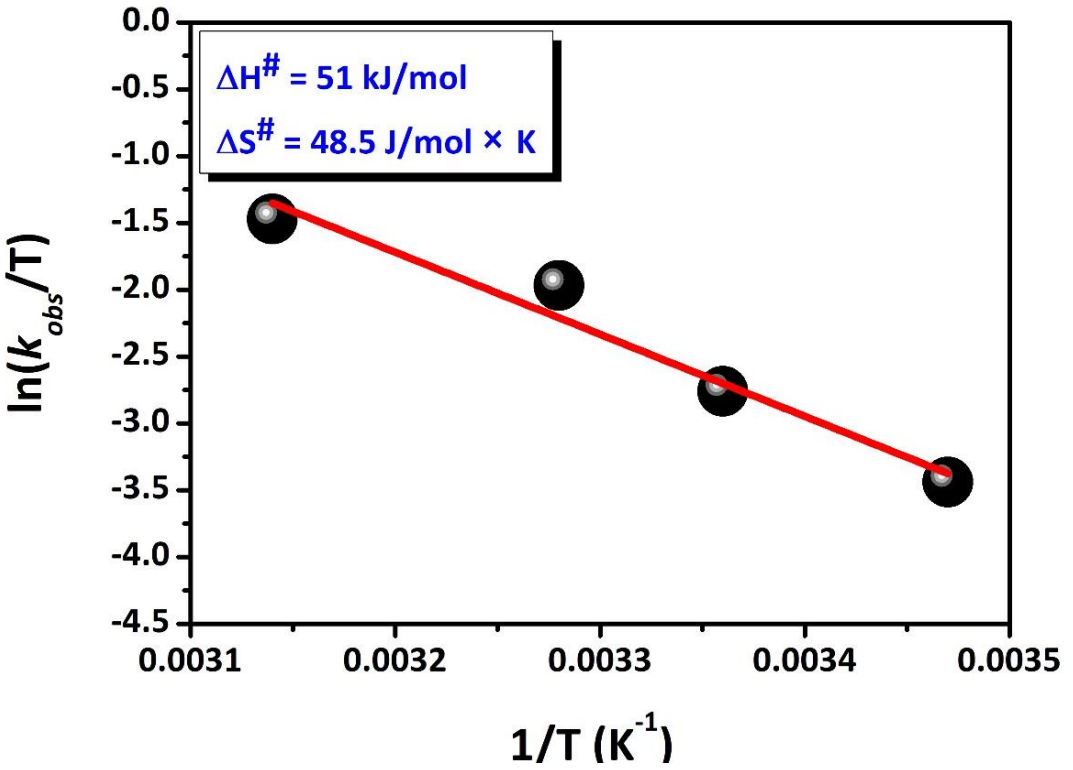

Figure S3. Eyring curve.

References

S1. Gunderloy FC. Hydrazine-mono- and bisborane. Inorg Synth 1967; 9: 13.

S2. Karataş Y, Gülcan M, Şen F. Catalytic methanolysis and hydrolysis of hydrazine-borane with monodisperse Ru NPs@nano-CeO_2 catalyst for hydrogen generation at room temperature, Int J Hydrogen Energy 2019: 44: 13432-13442.

S3. Demirkan B, Kuyuldar E, Karataş Y, Gülcan M, Sen F. Ex situ synthesis and characterization of a polymer-carbon nanotube-based hybrid nanocatalyst with one of the highest catalytic activities and stabilities for the hydrolytic dehydrogenation of hydrazine-borane at room temperature conditions, J. Colloid Interface Sci. 2019; 552: 432-438.